# CFD Analysis of an Axial Fan for Mine Ventilation

Prepared for Parag Fans

ANSYS CFX Report # 30-1361-05-2513A

ANSYS Canada Ltd.
554 Parkside Drive
Waterloo, Ontario N2L 5Z4

Phone: (519) 886-8435
Fax: (519) 886-7580

http://www.ansys.com/cfx
cfx-info-na@ansys.com

Mar. 16, 2006

# Executive Summary

Parag Fans proposed to modle a fan system consisting of the intel, fan, and outlet components. This represented a significant increase in the complexity and knowledge required to perform the analyses in comparison to the previous experience that existed at Parag Fans

Four configurations of geometric variations were studied:

1) Fan only (2.5 mm tip clearance)
2) Fan only (5 mm tip clearance)
3) Fan with guide vanes and conduit
4) Fan with guide vanes, conduit, and support struts

The results for total pressure were found to be within 1% of the design data prediction. Efficiencies were found to be slightly higher than the design data due the reduced torque on the blade calculated by the CFD analysis. The impact of the various geometric simplifications was also recorded.

ANSYS DesignModeler was used for geometry creation of the inlet, guide vane, and outlet sections, while CFX-TurboGrid was used for the fan blade geometry creation and meshing. CFX-Mesh was used to mesh the remaining components. CFX-10.0 was used for all CFD calculations.

# Disclaimer

Parag Fans assumes all professional engineering responsibility connected with the use of this result. ANSYS Canada Ltd. Makes no representation with respect to the adequacy of the result contained in this report, for any particular purpose or with respect to its adequacy to produce any particular result. Parag Fans acknowledges that the result contain modeling assumptions and that the result are not made of this Report or any other report, materials, equipment, or information arising from, or related to, the work described herein either by Parag Fans or any third party.

| **ANSYS Reference:** | |
|---|---|
| Project Number: | 30-1361 |
| Quote Number: | 05-2513 |
| Report Number: | 30-1361-05-2513 |
| Date: | Mar. 16, 2006 |

This report written by:

Bill Holmes
CFD Applications Specialist

Refereed by:

Kevin Matsui
Manager, Consulting and Technical Support

# Contents

# 1. Introduction

The key objective of this project was to perform a steady state CFD analysis on an axial fan intended for use in an exhaust air application for an underground mining installation. M & I had prior experience modelling the inlet and outlet components of a fan system, however they desired to increase their capability to include modelling of the actual fan. This represented a significant increase in the complexity and knowledge required to perform the analyses in comparison to the previous experience that existed at Prag Fans.

It was expected that the knowledge gained through this project and augmented in supplementary training would accelerate the capabilities of M & I to be able to model complete fan systems as part of their skill set.

The fan was a 10 bladed , 38" diameter axial fan intended for use in an exhaust air application for an underground mining installation. Four cases in different configurations were studied:

1) Fan only (2.5 mm tip clearance)
2) Fan only (5 mm tip clearance)
3) Fan with guide vanes and conduit (Shown in Figure 1.1)
4) Fan with guide vanes, conduit, and support struts

For all CFD simulations in this study, the CFX 10.0 computational fluid dynamics software was employed. The CFX 10.0 flow solver is a finite element based control volume method, which solves the three-dimensional Reynolds-averaged Navier-Stokes equations for fluid flow within complex geometries.

In this report a brief overview of the pre-processing methods will be presented, and a detailed discussion of the simulation methods and results will be presented.

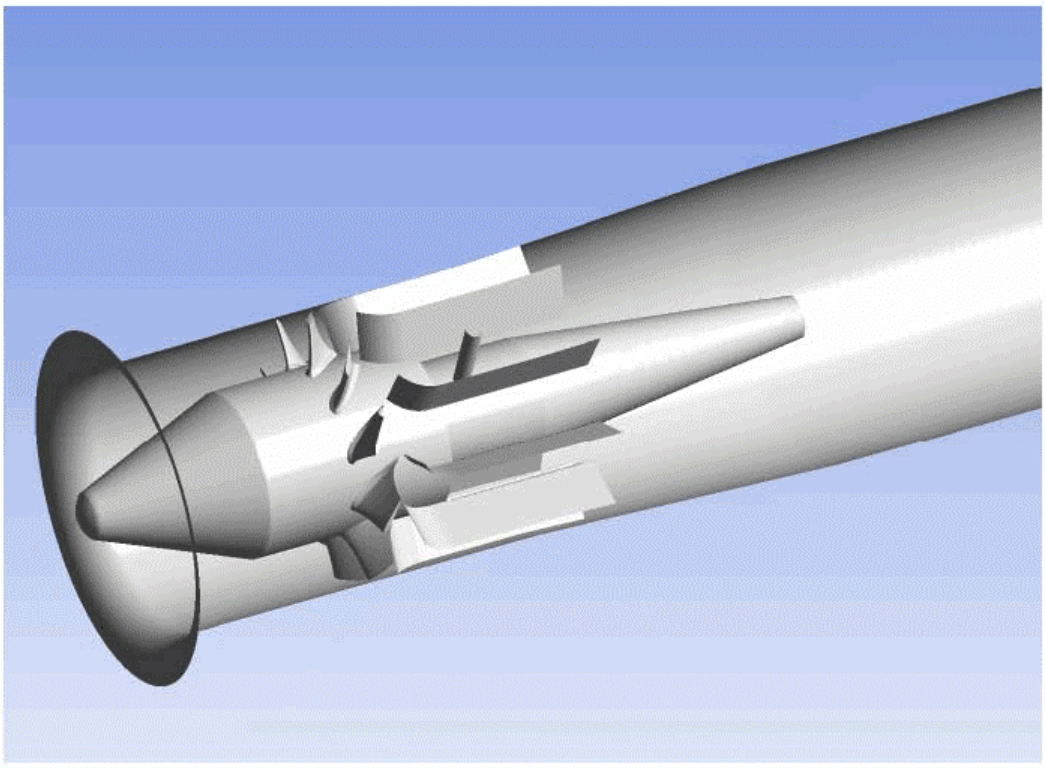

**Figure 1.1: Fan model (with guide vanes and conduit) for CFD study.**

## 2. Pre-Processing: Geometry

M&I Air supplied a number of 2D prints that were used to create the geometry for the computational model. In addition, a file containing the blade cross section points was sent to facilitate model creation in CFX-TurboGrid.

Four domains were modeled for this study and are shown in Figure 2.1 below: The inlet domain (red), the fan domain (yellow), the (interchangeable) stator domain (blue), and the outlet diffuser domain (green).

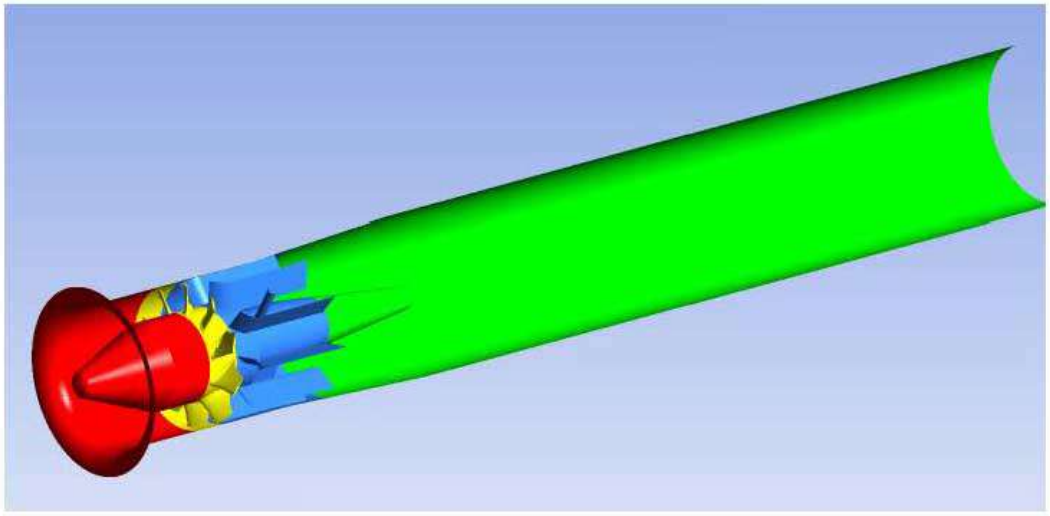

**Figure 2.1: Geometry used for CFD Study**

## 2.1. Inlet Geometry

The inlet domain was created using DesignModeler. The inlet model contained the inlet bellmouth, as well as a section of the ducting leading up to the fan. A hemisphere protruding out into the fluid domain was created to define the inlet to the domain. A 36 degree section representing one tenth of the entire section was used for the study.

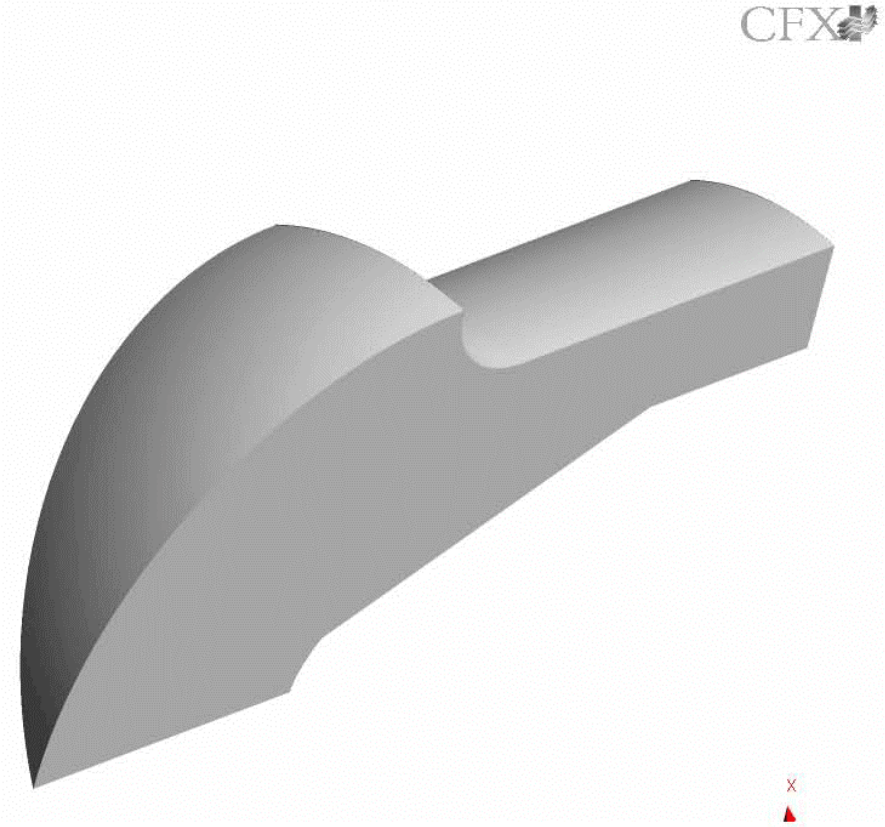


**Figure 2.2: Inlet Geometry**

## 2.2. Fan Blade Geometry

The blade profiles provided were imported into TurboGrid. The fan was modeled with a 2.5 mm and a 5 mm tip clearance. One blade passage was modeled for this study. The blade was rotated so that the blade tip camber line angle was 27° as measured from axial. The full geometry is shown in Figure 2.3: the rotating hub and blades are shown in blue, and the non-rotating section of the hub is shown in grey. One assumption made for the fan domain, was that the fan was modeled attached completely to the hub. In reality, a small gap is present to allow the blades to be pitched at different angles. This modification was assumed to have little to no effect on the overall results.

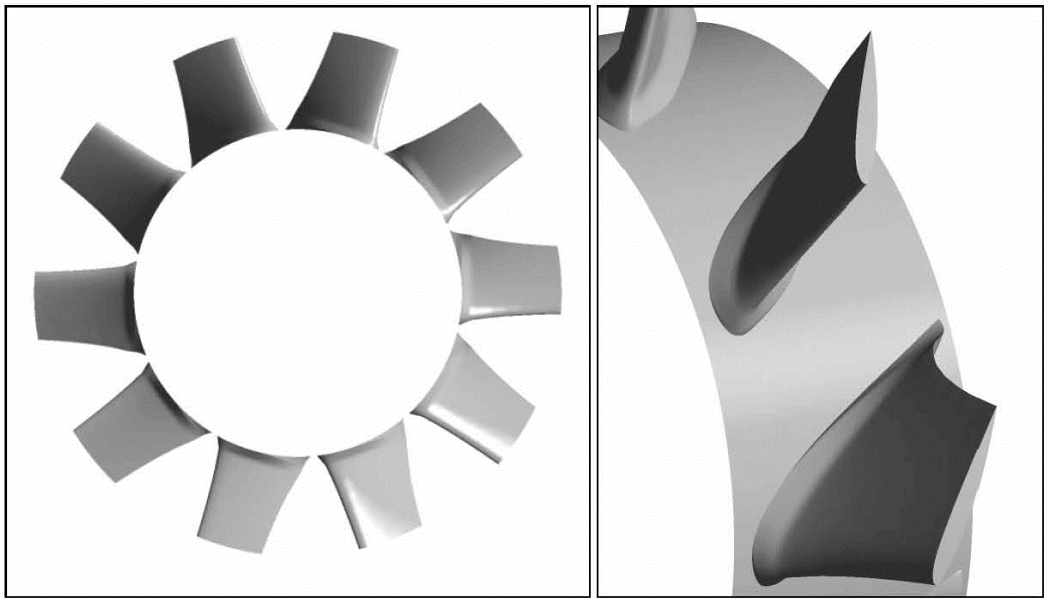

**Figure 2.3: Fan Blade Geometry**

Further modifications to the fan were proposed, namely reducing the hub length so that the blade trailing edge hung over the edge of the hub. Based on the complexity involved to model this feature, and based on the experience of ANSYS, these changes were deemed to be negligible and not included in the model.

## 2.3. Stator (Guide Vane) Geometry

The stator domain geometry was created in DesignModeler. The hub and shroud profile were provided by M&I Air in a DesignModeler file, and the stator geometry was provided by Canadian Buffalo in the form of 2-D prints. The stator row consisted of 9 guide vanes. Canadian Buffalo also provided information on the diameter and positions of the conduit and support struts. Three of the four support struts were modeled at 90° angles to each other, with the fourth offset

by 5° to avoid cutting through a stator vane. This change was necessary to facilitate meshing, and was assumed to be a minor change since the effect of the support struts was considered to be negligible. The conduit was located angularly between two of the 90° support struts.

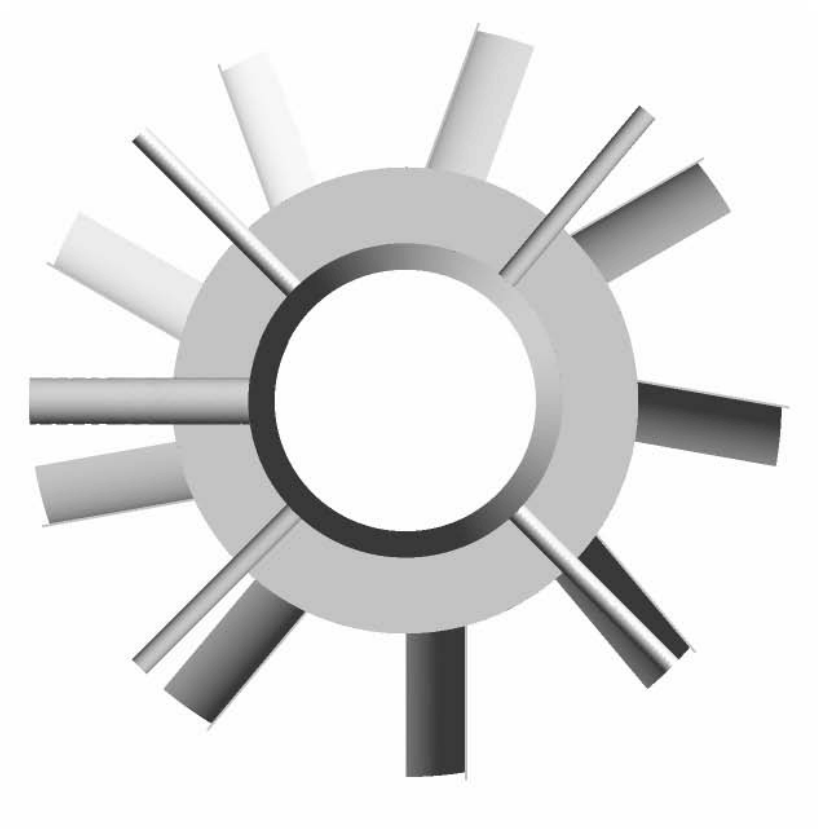

**Figure 2.4: Full Stator Domain Geometry shown from the outlet**

Three stator models were generated:

1) No stators, conduit, or support struts (modeled as 36° section)
2) Stator and conduit only (full 360° modeled)
3) Stator, conduit, and support struts (full 360° modeled)

Models 2 and 3 are shown in Figure 2.5 below.

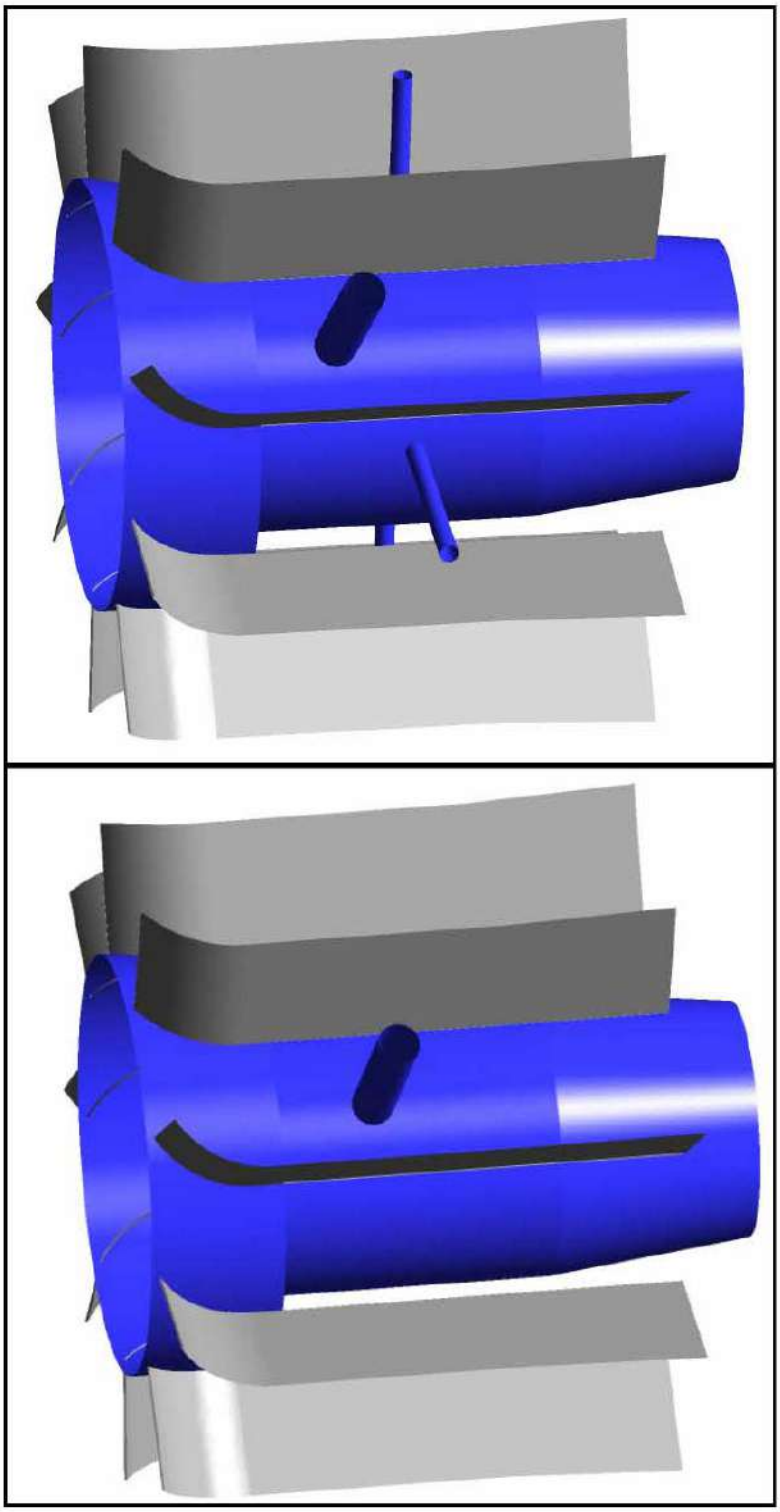

**Figure 2.5: Stator Vane Geometry Shown with (top) and without support struts**

## 2.4. Outlet Geometry

The outlet domain was created in DesignModeler. The outlet to the domain was defined as 200 inches downstream of the stator exit, as indicated in the ANSYS DesignModeler model provided by M&I Air. A 36° section of the outlet was modeled representing one tenth of the entire outlet domain for the case with no stators, conduit or support struts. The full 360° was modeled for the cases containing the non-axisymmetrical upstream components. The tail cone of the hub downstream of the stator vanes was included in the outlet domain.

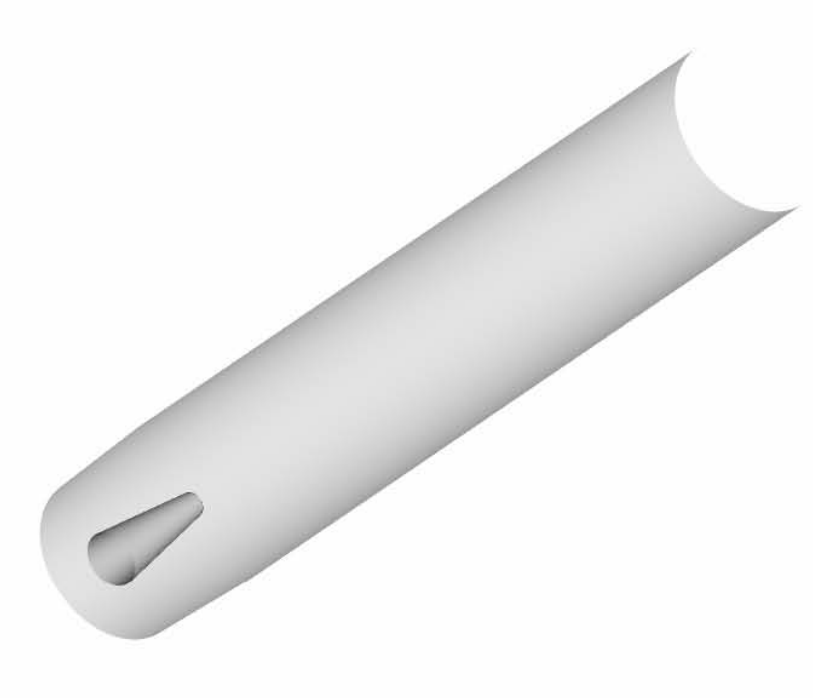

**Figure 2.6: Outlet Section Geometry**

## 3. Grid Generation

The computation grid used for the study was composed of a number of component meshes connected with a General Grid Interface (GGI) in CFX 10.0. The sizes of the meshes used in this study are shown in Figure 3.1 below.

| Mesh | Mesh Description | Number of Nodes | Number of Elements | Meshing Software |
|---|---|---|---|---|
| A | Inlet Domain (36° wedge) | 200336 | 443409 | CFX-Mesh |
| B | Fan Domain (2.5 mm gap) | 248106 | 233390 | TurboGrid |
| C | Fan Domain (5 mm gap, 36° wedge) | 249510 | 235000 | TurboGrid |
| D | Stator Domain (no stators, 36° wedge) | 150256 | 360812 | CFX-Mesh |
| E | Stator Domain with conduit (full 360°) | 1328817 | 3496377 | CFX-Mesh |
| F | Stator Domain with conduit and struts (full 360°) | 1424634 | 3786180 | CFX-Mesh |
| G | Outlet Domain (36° wedge) | 151213 | 336150 | CFX-Mesh |
| H | Outlet Domain (360° without struts) | 939445 | 2198805 | CFX-Mesh |
| I | Outlet Domain (360° with struts) | 826760 | 1876752 | CFX-Mesh |
| | Total for Run #1 (Meshes A,B,D,G) | 749911 | | |
| | Total for Run #2 (Meshes A,C,D,G) | 751315 | | |
| | Total for Run #3 (Meshes A,B,E,H) | 2716704 | | |
| | Total for Run #4 (Meshes A,B,F,I) | 2699836 | | |

**Figure 3.1: Mesh Sizes used for Study**

The inlet, stator and outlet domains were meshed using CFX Mesh. These domains were meshed with an unstructured tetrahedral mesh with an inflation layer along the hub and shroud surfaces. Inflation layers were also included on the stator, conduit, and support strut surfaces when these components were included in the mesh.

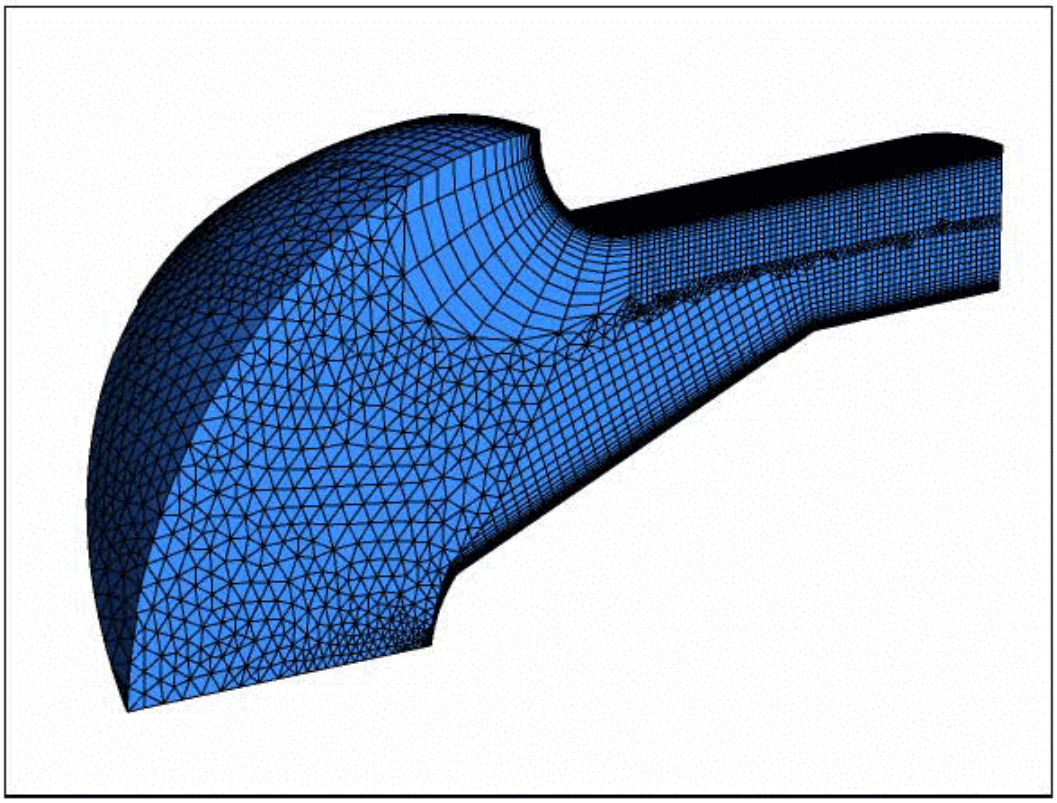

**Figure 3.2: Inlet Domain Mesh**

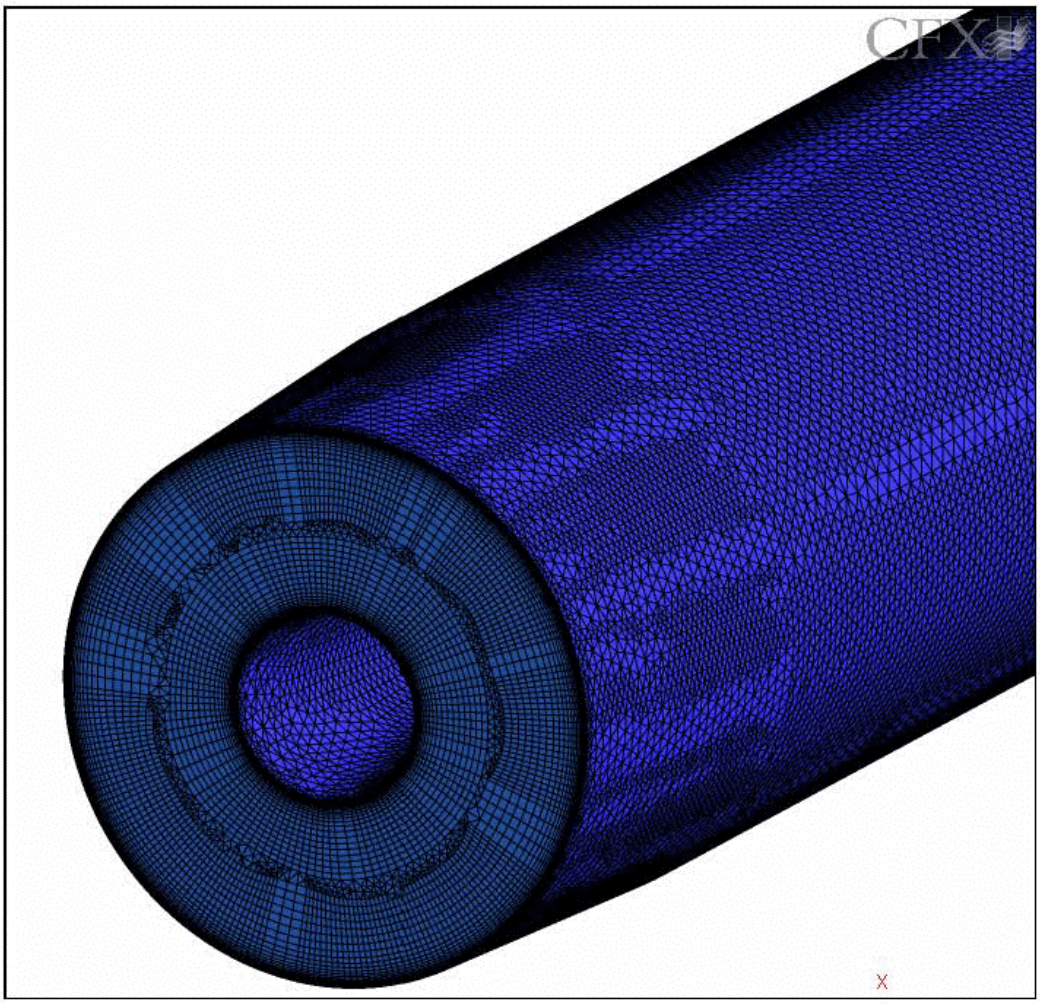


**Figure 3.3: Outlet Domain Mesh**

The mesh around the fan blade was generated using CFX-TurboGrid. The fan blades were meshed with a structured hexahedral mesh with an inflation layer around the blade and along the hub and shroud surfaces. The tip gap of 2.5 mm and 5 mm were modeled for the fan blades.

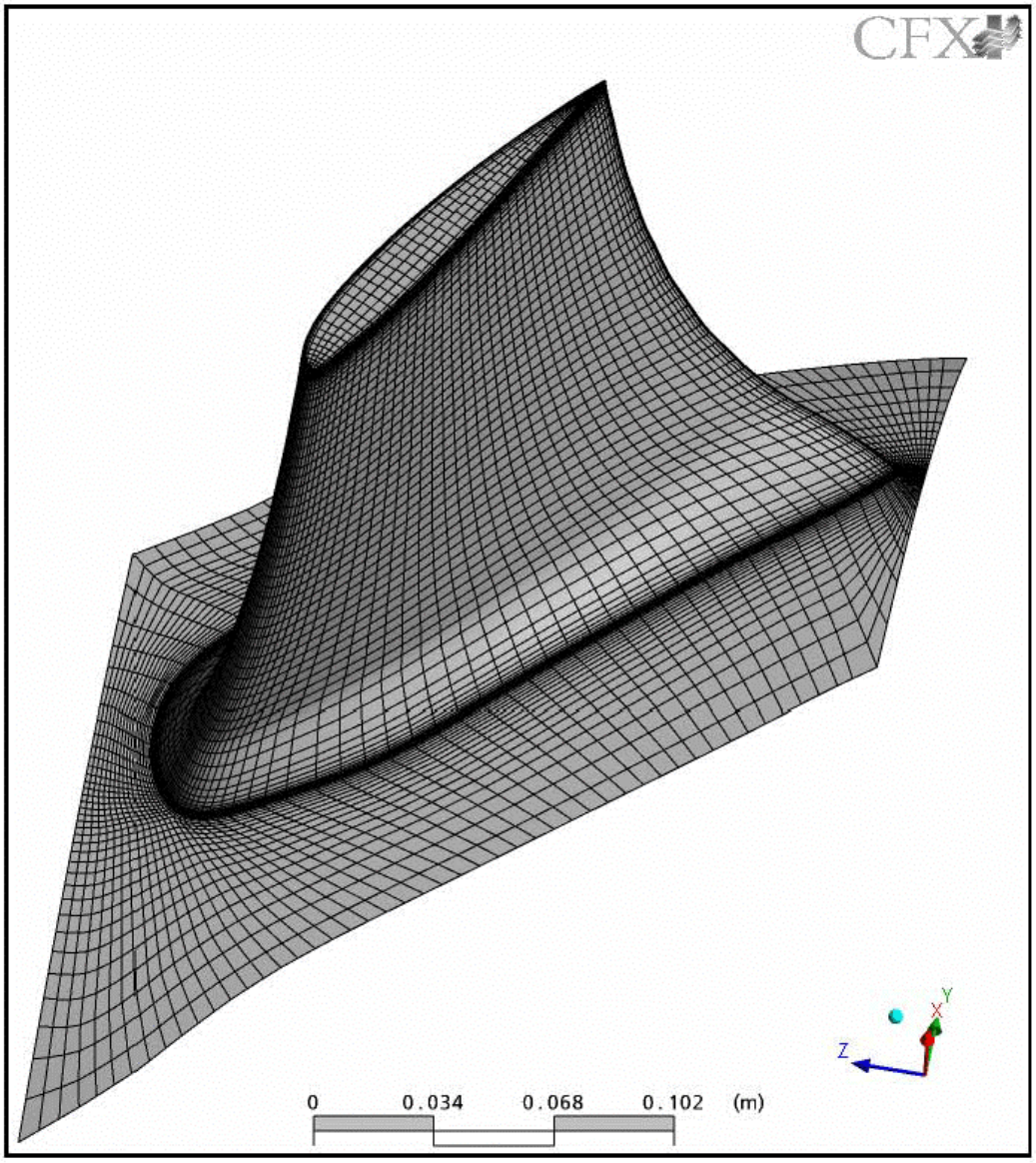


**Figure 3.4: Mesh on Hub and Blade Surfaces**

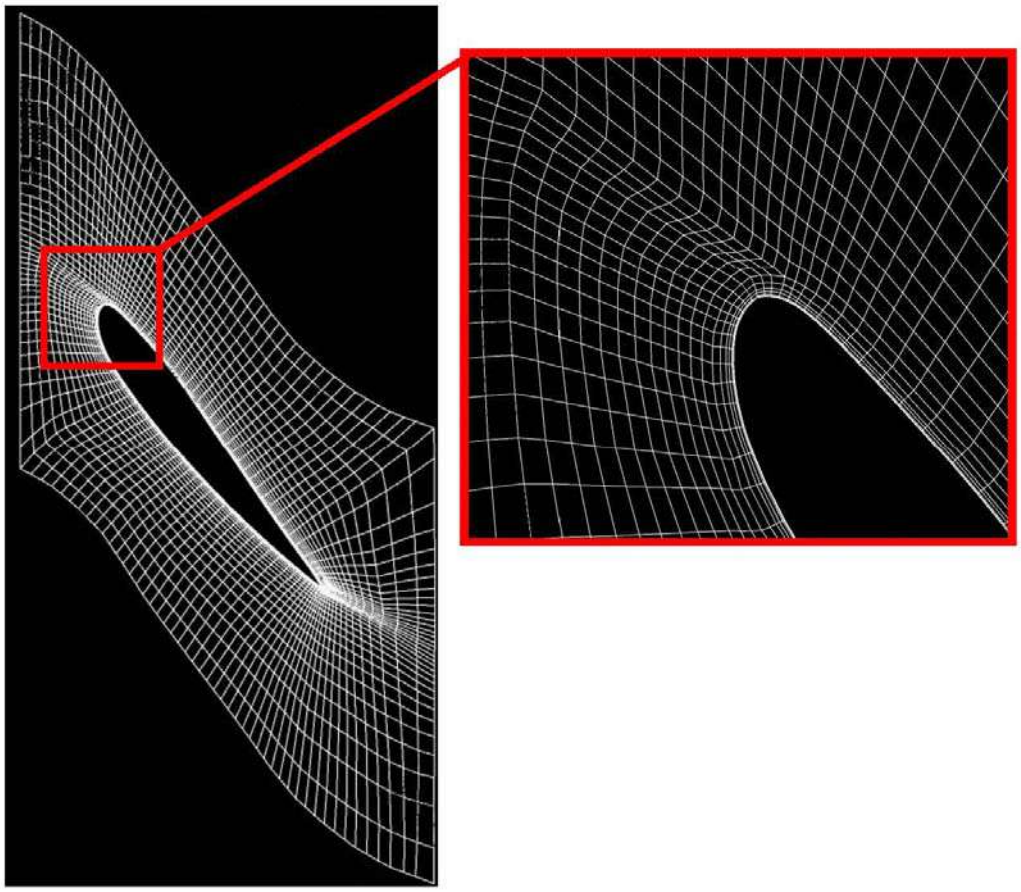

**Figure 3.5: Mesh at Approx. 50% Span**

The stator domain was meshed using CFX-Mesh. The stator vanes were meshed with an unstructured tetrahedral mesh with an inflation layer around the vane and along the hub and shroud surfaces. The conduit and support struts also had inflation layers when present.

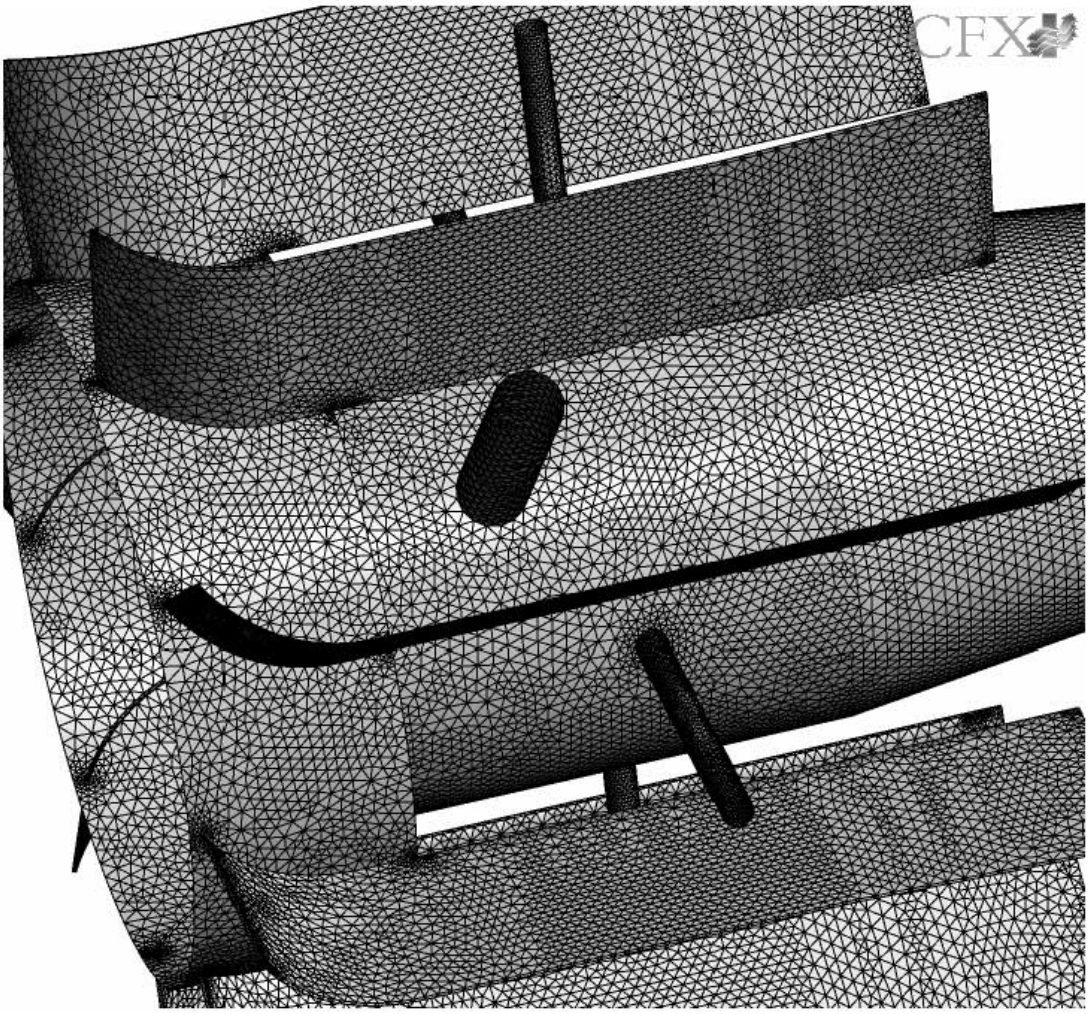


**Figure 3.6: Stator Mesh on Hub, Conduit, Support Strut, and Vane Surfaces**

## 4. Physical Properties and Boundary Conditions

The fluid used for the simulation was Air at 25°C and 1 atm with a density of 1.2 kg/$m^3$.

A summary of the operating conditions is listed in Figure 4.1 for quick reference.

| | |
|---|---|
| Inlet Total Pressure | 0 Pa |
| Outlet mass flow | 14.158 $m^3$/s |
| Number of Fan Blades | 10 |
| Number of Stator Vanes | 9 |
| Fan Diameter | 0.965 m |
| Fan Hub Diameter | 0.6 m |
| Interface between fan domain and stator domain | Stage |
| Interface between inlet domain and fan domain | Frozen Rotor |
| Interface between stator domain and outlet domain | None (no frame change) |
| Rotational Speed | 1760 rpm |
| Turbulence Model | K-Epsilon |

**Figure 4.1: Summary of Operating Conditions**

### 4.1. Computational Domain

**Domains:**
All domains were defined with a reference pressure of 1 atm and a fluid reference temperature of 25°C. The standard K-Epsilon turbulence model with scalable wall functions was employed. The fan domain was defined as rotating with a rotational speed of 1760 rpm, and the other three domains were defined as stationary domains.

**Inlet Boundary:**
The inlet boundary was defined as a Total Pressure boundary with a relative pressure of 0 Pa. Flow direction specified as normal to the hemispherical inlet surface.

**Outlet Boundary:**
The outlet boundary was defined as a mass flow exit with a mass flow of 1.69896 kg/s. Since only 1/10 of the full periodic section was modeled, this represents one tenth of the total mass flow through the machine (16.9896 kg/s). The mass flow was calculated by multiplying the volume flow rate (14.158 $m^3$/s) and the density of (1.2 kg/$m^3$).

**Wall Boundaries:**
The fan blade and fan hub walls were defined as rotating, no slip walls. All other walls were defined as stationary, no slip walls.

**Periodic Boundaries:**
Four pairs of one to one node matching periodic boundaries were defined, one in each of the four domains.

## 4.2. Domain Interfaces

Three General Grid Interfaces (GGI) were used to connect the four domains: one interface between the inlet and fan domains, one interface between the fan and stator domains, and one interface joining the stator and outlet domains. The GGI allows for surface meshes of dissimilar mesh distribution to be attached. The numerical algorithms employed in CFX are designed and implemented in such a way as to provide maximum robustness and accuracy. The treatment of the interface fluxes is fully implicit and fully conservative in mass, momentum, energy, scalars, etc.

The interface connecting the inlet and fan domains was defined as a frozen rotor interface. The frozen rotor allows for a frame of reference change across the interface, but the relative orientation of the components across the interface is fixed. This model produces a "steady state" solution to the multiple frame of reference problem, with some account of the interaction between the two frames. A perfect pitch ratio of 1 was used since the both the inlet domain and the fan domain consisted of a 36 degree section.

The interface connecting the fan and stator domains was defined as a stage interface. Flow moving across this interface was circumferentially averaged. The stage averaging between blade passages accounts for time average interaction effects, but neglects transient interaction effects.

In the cases modeled with stators, a pitch change of 0.1 was used since the fan domain consisted of a 36° section and the stator domain consisted of a full 360° degree section. The full 360° of the downstream components was modeled since the conduit and support struts are not symmetrical about the axis.

In the cases modeled with the fan only (no stators), a pitch change of 1 was used since both the upstream and downstream components consisted of a 36° sector.

A GGI was used to join the stator and outlet domains, with the frame change option set to none. No pitch change is necessary for this type of interface, since the upstream and downstream sides of the interface in the same frame of reference.

In addition, a GGI was used on the surface in the tip gap region that extends from the blade mid-surface line at the tip to the shroud wall. This surface is created by default in CFX-TurboGrid to allow tip clearance meshes to be formed without having to match nodes across the blade thickness. This interface is shown in Figure 4.2.

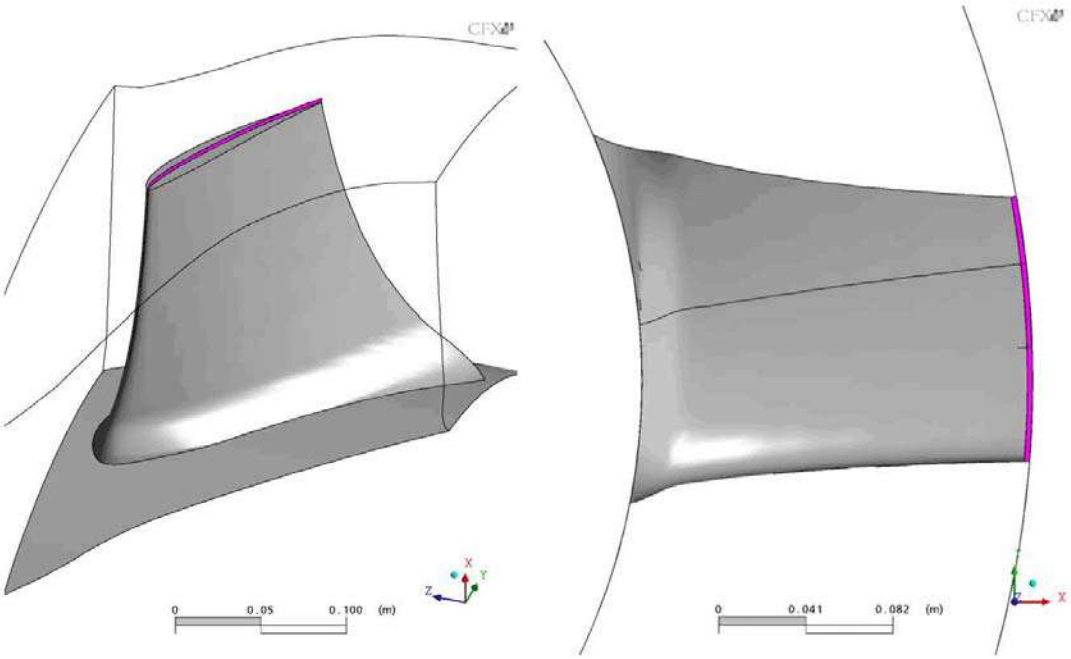


**Figure 4.2: GGI in Tip Clearance Region**

# 5. Results

## 5.1. Convergence

The maximum RMS residuals for the momentum terms were less than 1.7e-5 for the three cases with the 2.5 mm tip clearance, and less than 2.2e-4 for the case with the 5 mm tip clearance. All mass and momentum imbalances for all four CFD runs were below 0.0053%. The total efficiency was also monitored to ensure the case was fully converged.

## 5.2. Tabulated Values

A number of variables were calculated in CFX-Post, and these values were tabulated, and are shown in Figure 5.1 below.

Fan Information - M&I Air

| Description | Units | Design Data | 2.5 mm gap, fan only | 5 mm gap, fan only | With Guide Vanes, Conduit | With Guide Vanes, Conduit, Support Struts |
|---|---|---|---|---|---|---|
| *Fan Diameter* | m | 0.965 | 0.965 | 0.96 | 0.965 | 0.965 |
| *Hub Diameter* | m | 0.6 | 0.6 | 0.6 | 0.6 | 0.6 |
| *Shroud Diameter* | m | | 0.97 | 0.97 | 0.97 | 0.97 |
| *Number of Blades* | | 10 | 10 | 10 | 10 | 10 |
| *Density* | kg m^-3 | 1.2 | 1.2 | 1.2 | 1.2 | 1.2 |
| *Flow Rate (Q)* | m^3 s^-1 | 14.158 | 14.158 | 14.158 | 14.158 | 14.158 |
| *Fan Speed* | radian s^-1 | | 184.3 | 184.3 | 184.3 | 184.3 |
| *Fan Speed* | RPM | 1780 | | | | |
| | | | | | | |
| *Overall Quantities* | | | | | | |
| *Delta Pt* | Pa | | 1148.9 | 1075.5 | 1241.6 | 1224.7 |
| *Delta Ps* | Pa | | 882.8 | 818.6 | 1135.4 | 1118.3 |
| *Total Efficiency* | | | 67.4% | 63.5% | 73.1% | 72.1% |
| *Static Efficiency* | | | 51.8% | 48.4% | 66.8% | 65.8% |
| | | | | | | |
| | | | | | | |
| *Fan Only Quantities* | | | | | | |
| *Delta Pt* | Pa | 1471 | 1479.1 | 1394.9 | 1451.8 | 1451.0 |
| *Delta Ps* | Pa | 873.09 | 1266.6 | 1176.3 | 1299.5 | 1298.7 |
| *Total Efficiency* | | 82.6% | 86.8% | 82.4% | 85.5% | 85.4% |
| *Static Efficiency* | | 49.0% | 74.3% | 69.5% | 76.5% | 76.4% |
| | | | | | | |
| *Fan Shaft Power* | W | 25230 | 24122 | 23964 | 24052 | 24053 |
| *Tip Gap* | mm | | 2.5 | 5 | 2.5 | 2.5 |

**Figure 5.1: Fan Performance Values**

Pressures and efficiencies are given as "overall quantities" and as "fan only quantities". The overall quantities are defined using the pressure measured at the inlet to the domain and the outlet of the domain. The fan only quantities were determined using the pressure at the inlet to the fan domain and the outlet to the fan domain (i.e. the GGI interfaces). The planes used to calculate the fan only values are shown in

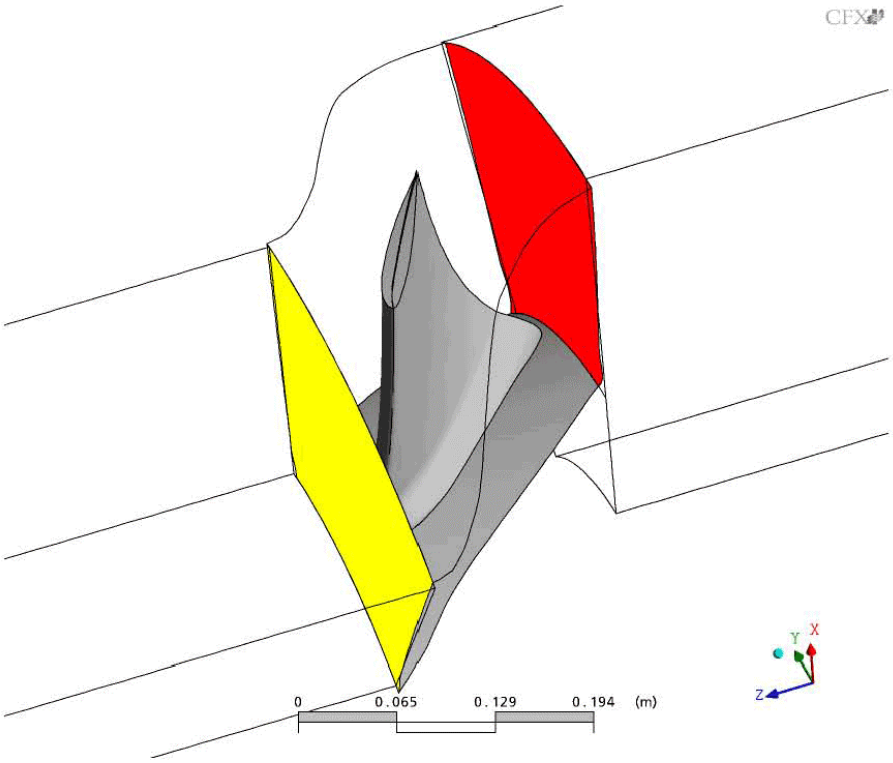


**Figure 5.2: Planes used for Fan Only measurements**

The total pressure rise was calculated by taking the difference between the mass-averaged total pressure at the outlet (where the diffuser begins the transition from a circular cross section) and the mass-averaged total pressure on a plane at the inlet of the bellmouth. The static pressure rise was calculated by taking the difference between the mass averaged static pressure on the same

planes mentioned above. The total efficiency ($h_t$) calculation used for the table calculations were:

$$\eta_t = \frac{\Delta P_t * Q}{N * T}$$

where Q is the volumetric flow rate at the outlet in $m^3/s$, T is the torque measured on the fan surfaces in N*m, and N is the rotational speed in rad/s.

$$\Delta P_t = P_{tOUTLET} - P_{tINLET}$$

The torque was calculated from the change in angular momentum at the inlet compared to the outlet. The torque, T, is given by the following equation:

$$T = \dot{m}(rV_{\theta,OUTLET} - rV_{\theta,INLET})$$

where r is the radius of each particular element on the blade surface and $V_\theta$ is the tangential velocity at each node on the corresponding location. For example, the $rV_{\theta,OUTLET}$ component is calculated by determining r* $V_\theta$ at every node on the fan ? outlet surface, and then mass averaging these value over the entire surface.

### 5.3. Discussion of Results – Fan Only

The total pressure was plotted in the inlet section to determine the losses in this region. This plot is shown in Figure 5.3, and the total pressure loss is minimal in this section as suspected.

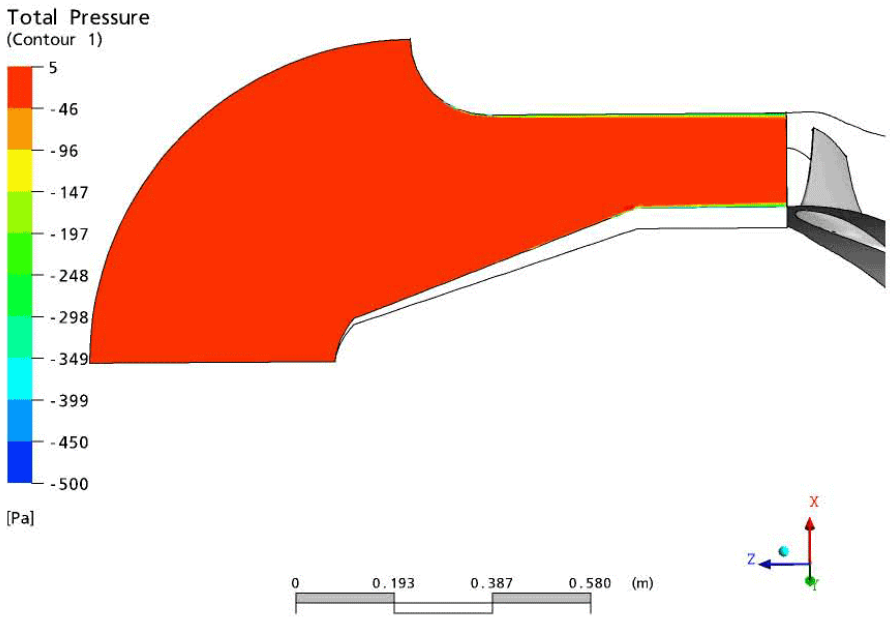


**Figure 5.3: Total pressure on periodic plane of inlet section.**

The blade design appears to be quite efficient. The relative total pressure loss through the blades is minimal (as shown in Figure 5.4), and the flow stays attached to the blade resulting in a small wake (as shown in Figure 5.5). Figure 5.4 depicts the relative total pressure through a plane at mid-span of the blade (i.e. Half the distance between the hub and the blade tip). A velocity vector plot is shown in Figure 5.5, which shows the flow around the blade in the relative frame of reference to be mostly attached, with a small wake behind the trailing edge.

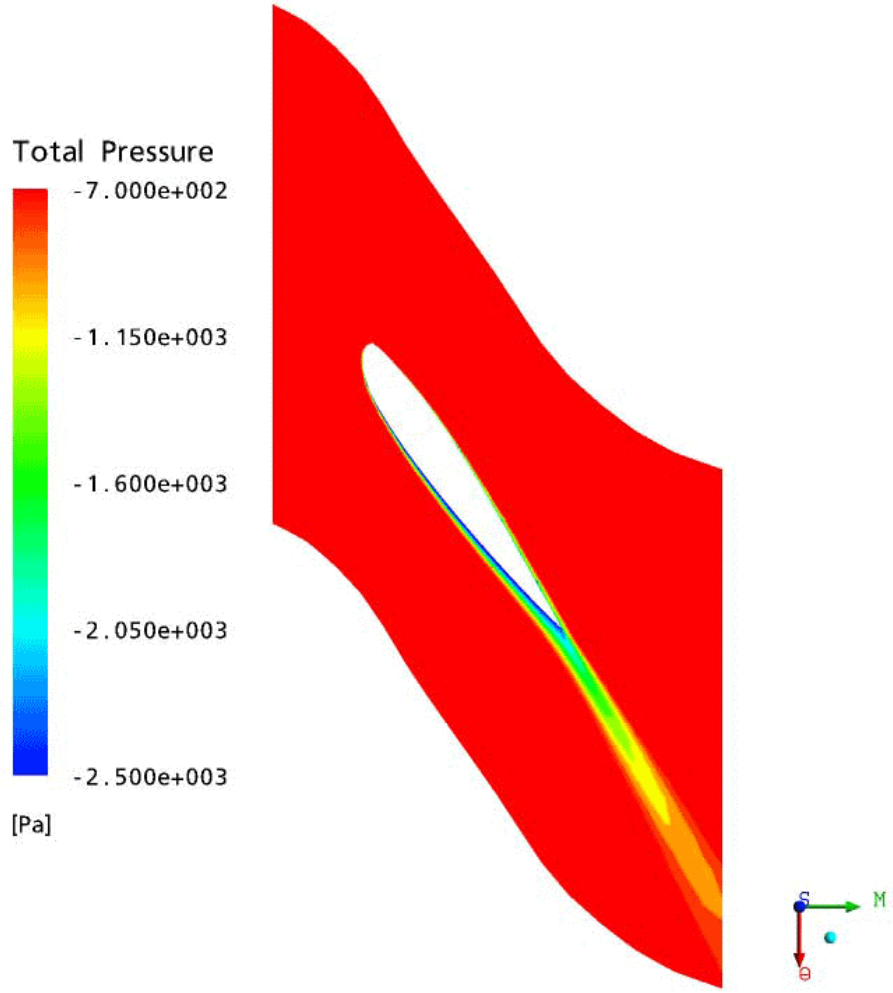


**Figure 5.4: Relative Total Pressure Contour in Blade Section at 50% Span.**

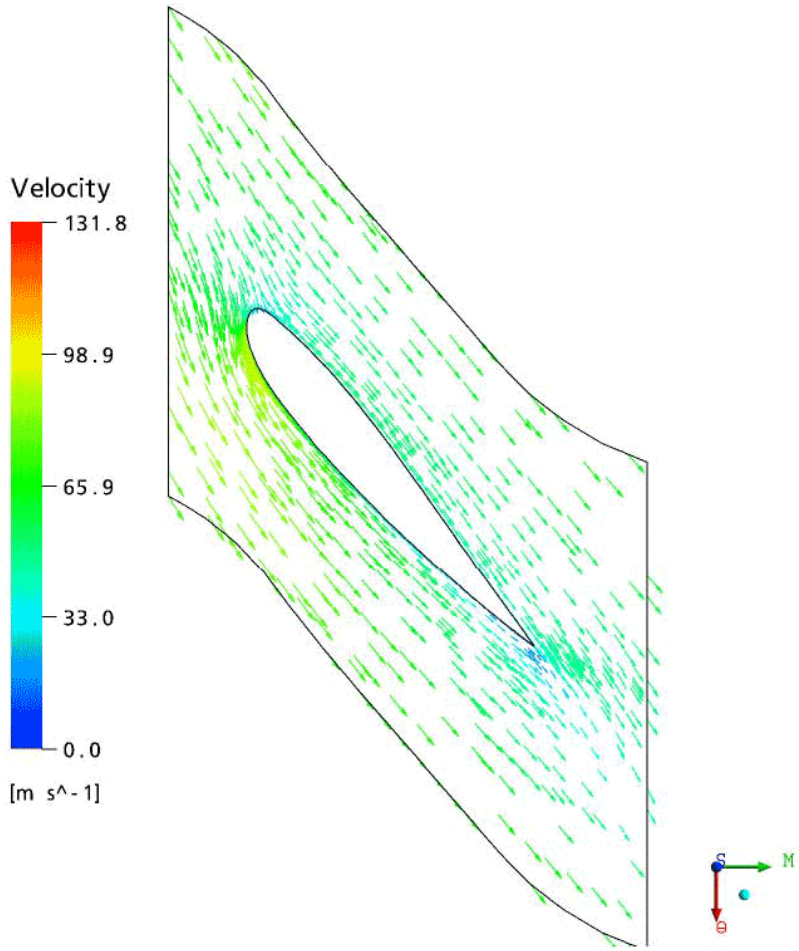


**Figure 5.5: Relative Velocity Vector in Blade Section Plot at 50% Span.**

In addition, some other plots of interest around the blade were generated and are shown below. The relative pressure values at 50% span are shown in Figure 5.6, and the streamlines in the relative frame of reference at the 50% span plane are shown in Figure 5.7. The circumferentially averaged flow angle was also plotted at the inlet to the fan domain in Figure 5.8.

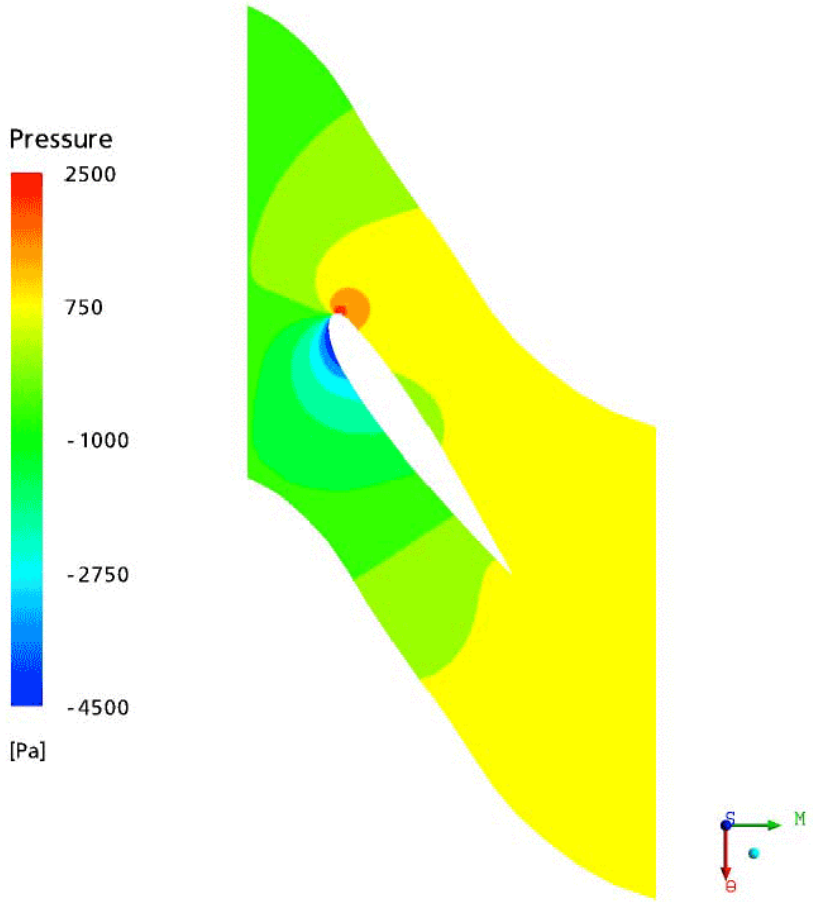


**Figure 5.5: Relative Pressure Contours in Blade Section at 50% Span.**

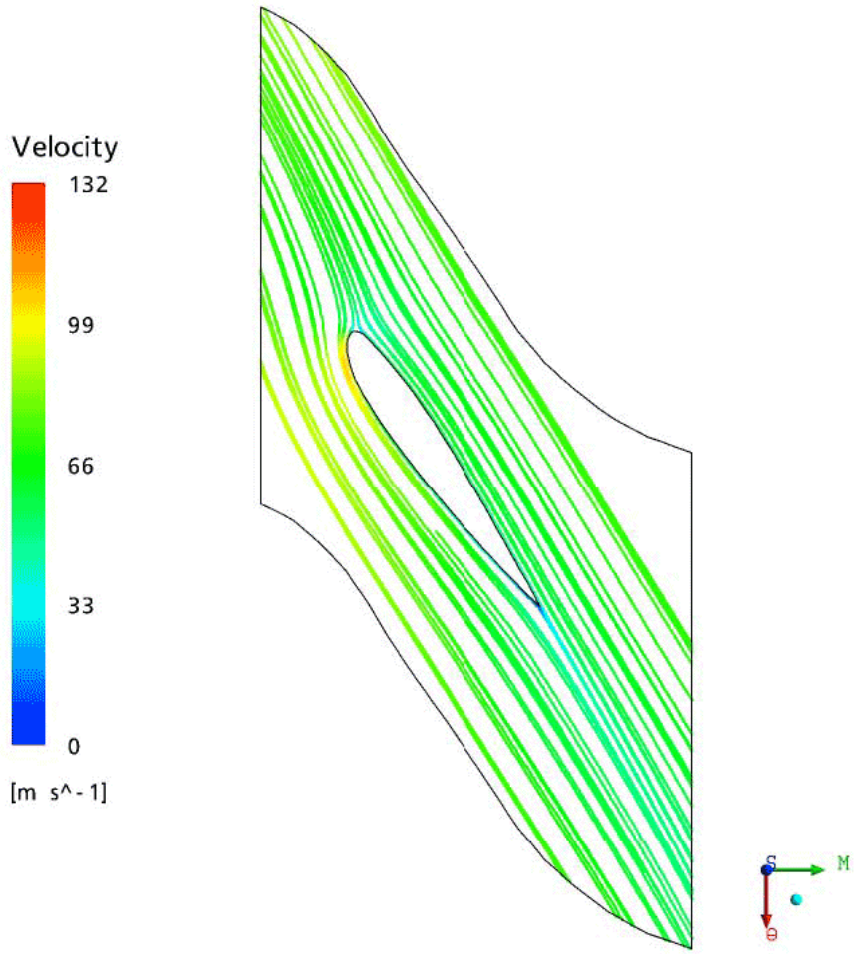


**Figure 5.7: Absolute Streamline Plot in Blade Section at 50% Span.**

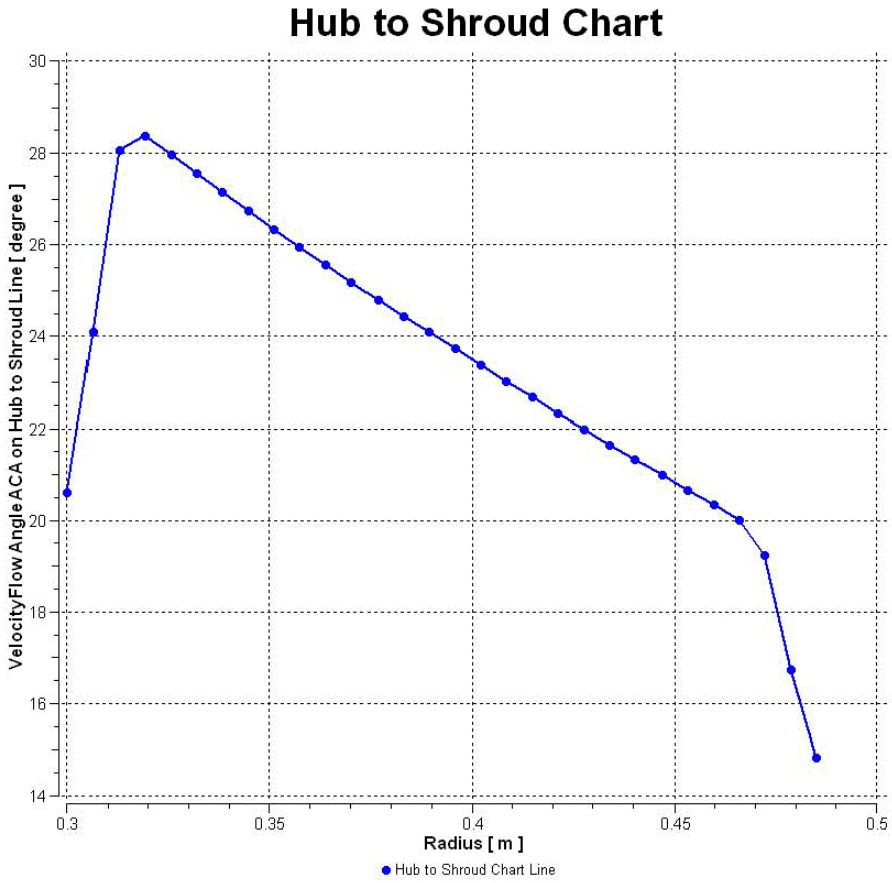


**Figure 5.8: Flow angle at fan inlet (fan pitch angle set to 27°).**

Overall the fan appears to be reasonably well designed, and designed to the desired load point. The downstream components were found to have little impact on the fan only calculations.

### 5.4. Discussion of Results – 2.5 mm vs. 5 mm tip clearance

The fan was modeled with two tip clearances to determine the effects of clearance on fan performance. The different geometries modeled are shown in Figure 5.9.

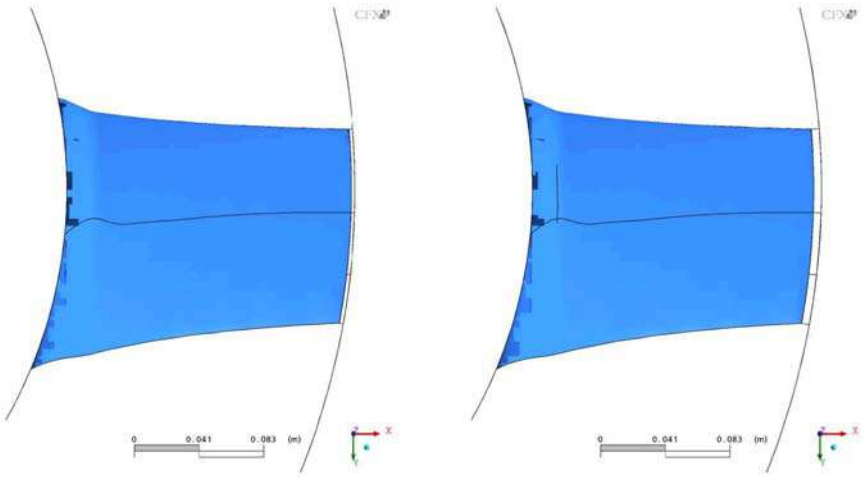


**Figure 5.9: Blade Geometry for 2.5 mm tip gap (left) and 5 mm tip gap (both from inlet side)**

Plots showing streamlines through the tip gap are shown in Figure 5.10. The tip vortex is noticeably stronger in the 5 mm gap case compared to the 2.5 mm case. The circumferentially averaged relative total pressure is plotted on a meridional plane for both cases in Figure 5.11. Again the larger reduction in total pressure in the tip region indicated the losses were greater for the 5 mm tip clearance case.

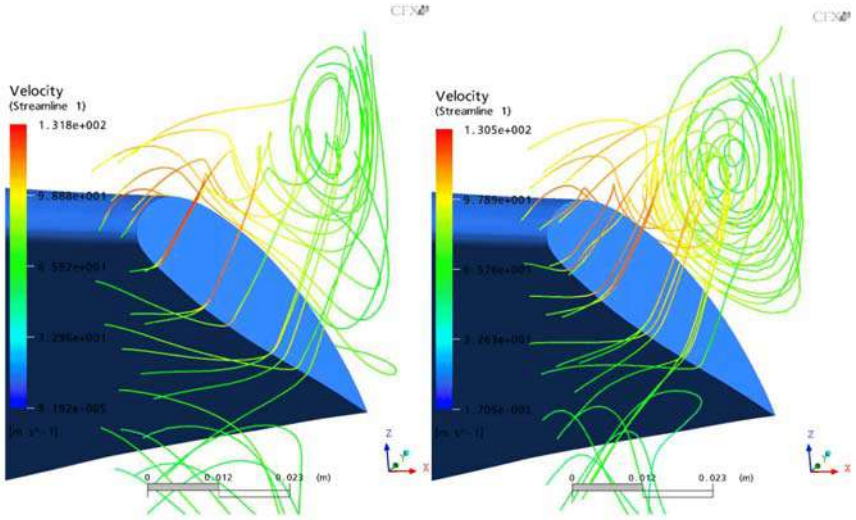


**Figure 5.10: Streamlines in gap for 2.5 mm tip gap (left) and 5 mm tip gap.**

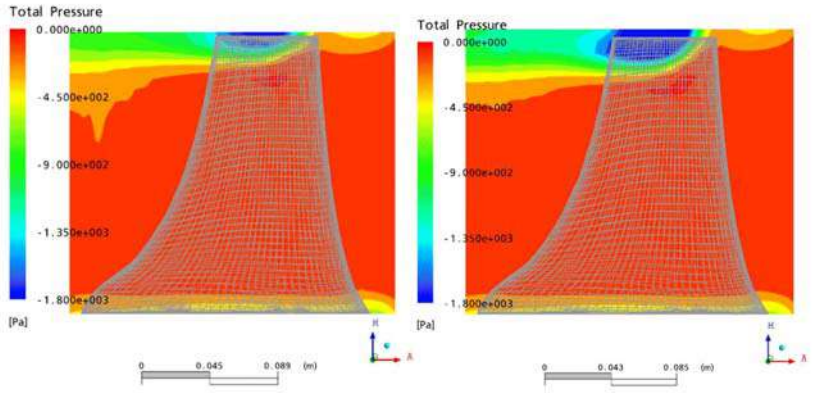


**Figure 5.11: Circumferentially averaged relative total pressure contour in meridional plane for 2.5 mm tip gap (left) and 5 mm tip gap.**

Based on computed results shown in Figure 5.11, the change in pressure due to the increase tip gap is significant. The 5 mm tip clearance resulted in an 84 Pa drop in total pressure rise generated by the fan compared to the 2.5 mm case (5.7% decrease). The fan efficiencies also dropped by roughly 4.5%. The general consensus among the team members was that these levels were unacceptable, and that the remainder of the study should be completed with the 2.5 mm tip clearance.

| Description | Units | Design Data | 2.5 mm gap, fan only | 5 mm gap, fan only |
|---|---|---|---|---|
| *Fan Diameter* | m | 0.965 | 0.965 | 0.96 |
| *Hub Diameter* | m | 0.6 | 0.6 | 0.6 |
| *Shroud Diameter* | m | | 0.97 | 0.97 |
| *Number of Blades* | | 10 | 10 | 10 |
| *Density* | kg m^-3 | 1.2 | 1.2 | 1.2 |
| *Flow Rate (Q)* | m^3 s^-1 | 14.158 | 14.158 | 14.158 |
| *Fan Speed* | radian s^-1 | | 184.3 | 184.3 |
| *Fan Speed* | RPM | 1780 | | |
| | | | | |
| *Overall Quantities* | | | | |
| *Delta Pt* | Pa | | 1148.9 | 1075.5 |
| *Delta Ps* | Pa | | 882.8 | 818.6 |
| *Total Efficiency* | | | 67.4% | 63.5% |
| *Static Efficiency* | | | 51.8% | 48.4% |
| | | | | |
| | | | | |
| *Fan Only Quantities* | | | | |
| *Delta Pt* | Pa | 1471 | 1479.1 | 1394.9 |
| *Delta Ps* | Pa | 873.09 | 1266.6 | 1176.3 |
| *Total Efficiency* | | 82.6% | 86.8% | 82.4% |
| *Static Efficiency* | | 49.0% | 74.3% | 69.5% |
| | | | | |
| *Fan Shaft Power* | W | 25230 | 24122 | 23964 |
| *Tip Gap* | mm | | 2.5 | 5 |

**Figure 5.12: Tabulated results comparing 2.5 mm tip gap to 5 mm tip gap**

### 5.5. Discussion of Results – Support Struts

The examination of various plots around the stator region reveals that the stators are somewhat misaligned for this operating point. The flow impacts the stator at a negative incident angle, resulting in separation at the leading edge, as shown in the vector plot in Figure 5.13. The average flow angle entering the stator stage is 31°, and exits the stator stage at an angle of 4°. Note that a flow angle of 0° represents purely axial flow, and a flow angle of 90° represents purely tangential flow. The inlet stator blade angle was set to roughly 60°. This misalignment was responsible for the large separation of the leading edge, as shown in Figure 5.14. The resulting total pressure loss is also significant as shown in Figure 5.15. Potentially a larger radius on the stator would reduce the losses in this section and boost the static pressure at the outlet.

Based on the flow angle at the stator inlet and outlet, clearly the stators are removing the swirl component from the flow, and the resulting rise in static pressure is 360 Pa. The loss in total pressure over this section was 183.6Pa with stators and conduit only. Additional values are shown in Figure 5.16.

Additional plots showing the losses over the conduit and support struts are shown in Appendix A. Essentially the flow is what would be expected over a cylinder. The losses were less than 1% of the total pressure rise generated by the fan.

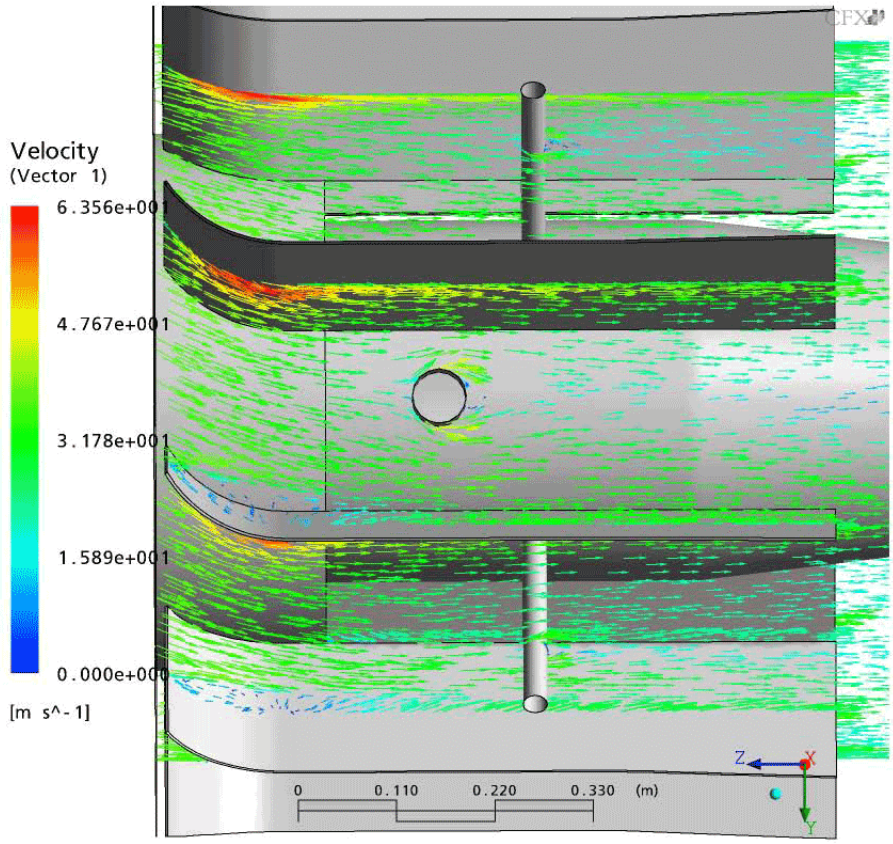


**Figure 5.13: Velocity Vector Plot in Stator Region at R=0.4m**

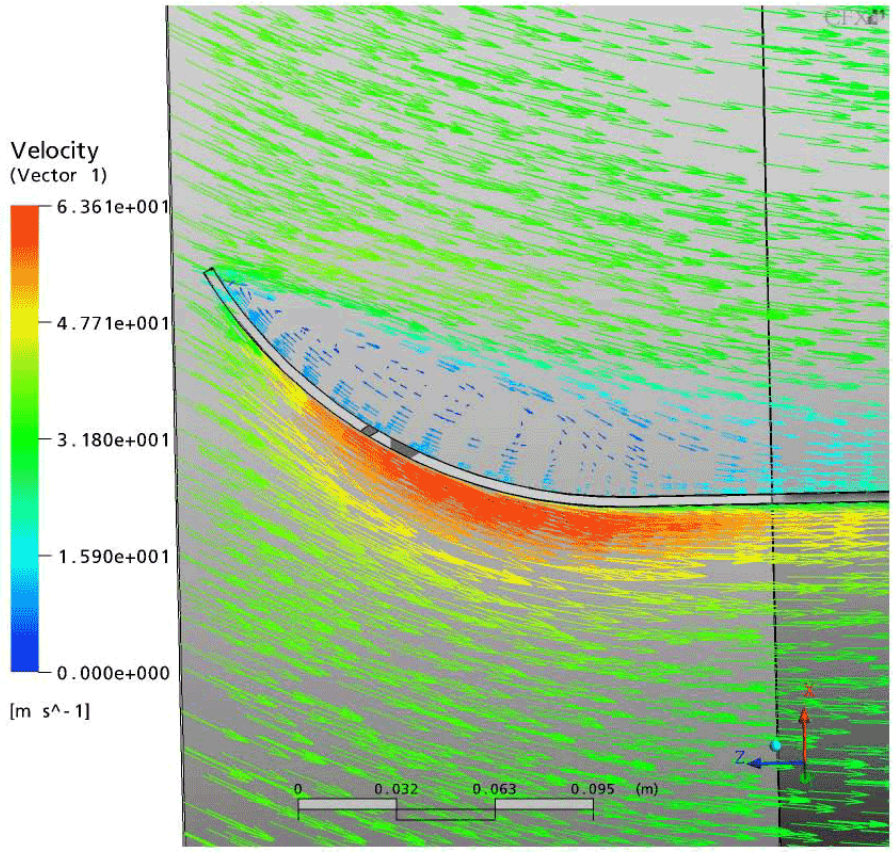


**Figure 5.14: Velocity Vector Plot at Stator Leading Edge at R=0.4m**

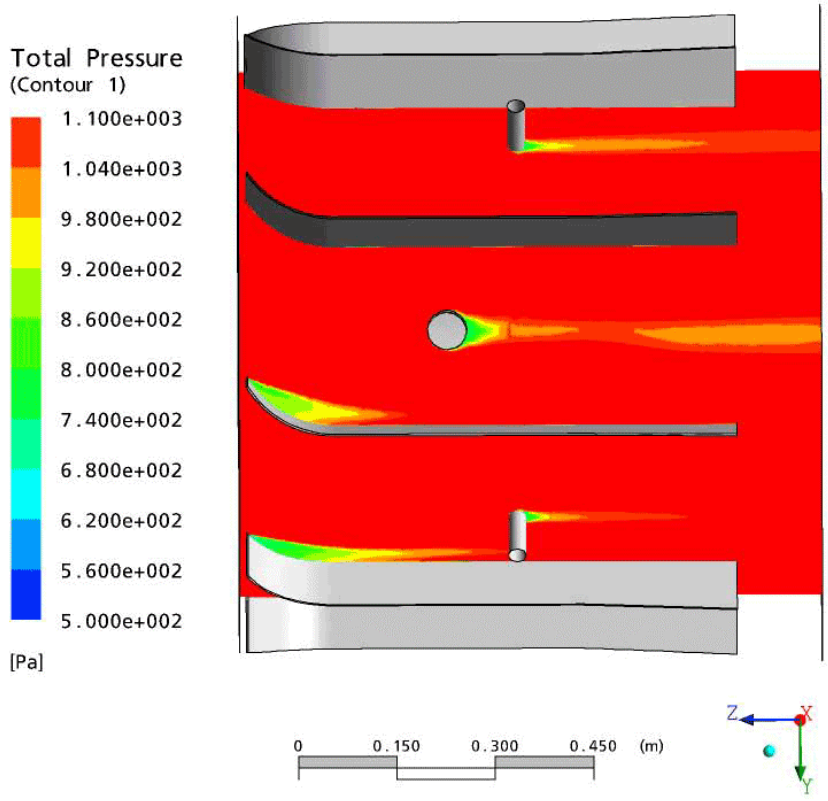


Figure 5.15: Total Pressure Plot in Stator Region at R=0.4m

| | With Strut | | Without Strut | |
|---|---|---|---|---|
| | Upstream | Downstream | Upstream | Downstream |
| Flow Angle | 31° | 4° | 31° | 4° |
| Total Pressure | 1437.2 Pa | 1235.5 Pa | 1437.1 Pa | 1253.5 Pa |
| Static Pressure | 621.4 Pa | 964.0 Pa | 621.3 Pa | 982.6 Pa |
| | | | | |
| Total Pressure Loss | 201.7 Pa | | 183.6 Pa | |
| Static Pressure Rise | 342.6 Pa | | 361.3 Pa | |

**Figure 5.16: Total Pressure Contours in Stator Region at 25% span**

Based on Figure 5.16, the addition of the four support struts does not affect the flow entering the stator stage. The struts do result in a total and static pressure reduction at the outlet of the stator stage by approximately 18 Pa compared to the case without struts. The struts were found to have no effect on the flow angle.

## 6. Conclusions

In summary, the fan was found to generate 1.479 kPa of total pressure at a fan speed of 1760 rpm and a volume flow rate of 14.158 m^3/s. The air density used in the case was 1.2 kg/m3, and the calculated total efficiency was 86.8% based on a shaft power of 24.122 kW. The total pressure and flow rate

The 5 mm tip clearance resulted in an 84 Pa drop in total pressure rise generated by the fan compared to the 2.5 mm case (5.7% decrease). The general consensus among the team members was that these levels were unacceptable, and that the remainder of the study should be completed with the 2.5 mm tip clearance.

The addition of guide vanes increased the outlet total pressure by 93 Pa (8.1% increase) and the outlet static pressure by 253 Pa (28.6% increase). The stators were found to improve the overall fan performance; however, a large amount of separation occurred at the leading edge, and recommendations on improving the design are included in the following section.

The addition of the support struts resulted in a decrease in both total and static pressure of 18 Pa (1.4% of the total pressure rise over the entire computational domain). The losses were quite small, and the resulting losses were found to be minimal should they be required in the installation.

Overall, the losses in the inlet and outlet section were found to be minimal. The fan blade seemed to be operating quite efficiently, with only a small wake behind the trailing edge and a small loss in relative total pressure. The stator design appeared to be misaligned with the flow, which contributed to total pressure losses through the stator stage.

## 7. Recommendations

The only major recommendation was to increase the camber radius of the stator so that the leading edge is better aligned with the flow. The average flow angle entering the stator was 31°, while the blade angle was set to roughly 60°.

## 8. References

1. *CFX-5 User Documentation Version 10.0*, ANSYS Canada Ltd., 2005.

## APPENDIX A: Additional Plots

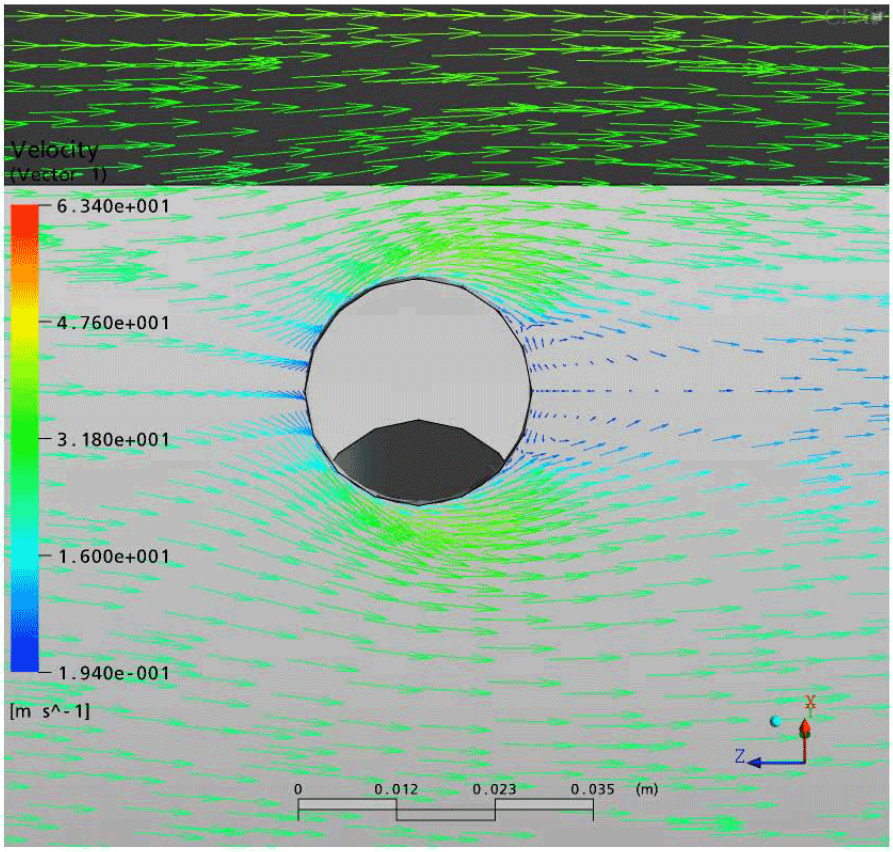


**Figure A1: Velocity Vector Plot near support strut at R=0.4m.**

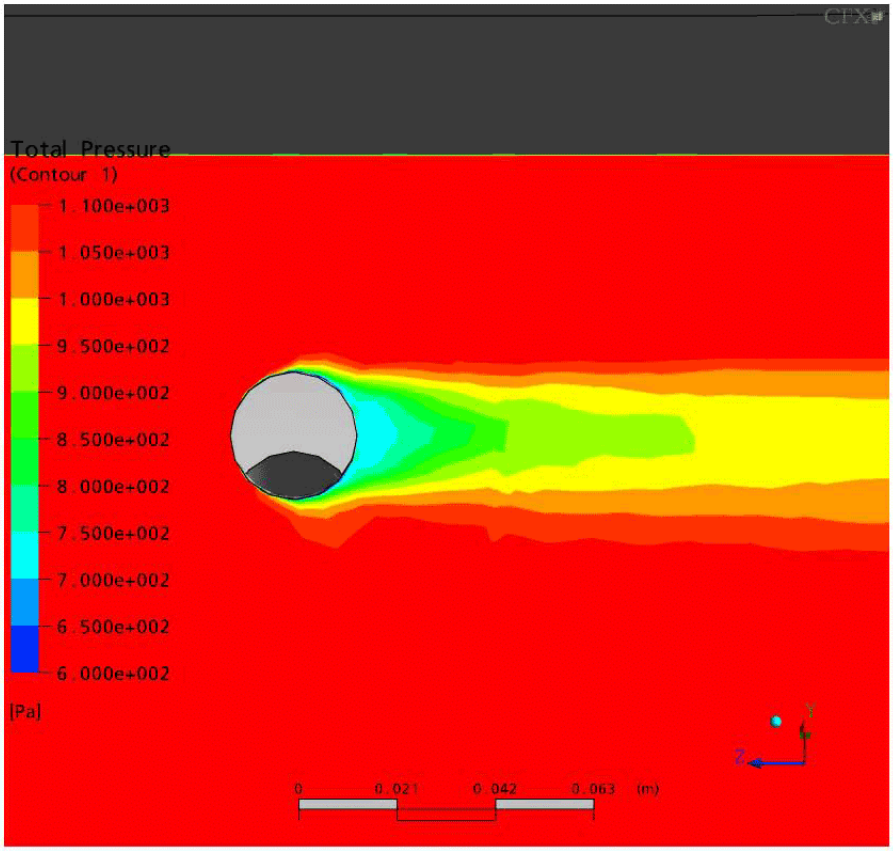


**Figure A2: Total pressure plot near support strut at R=0.4m.**

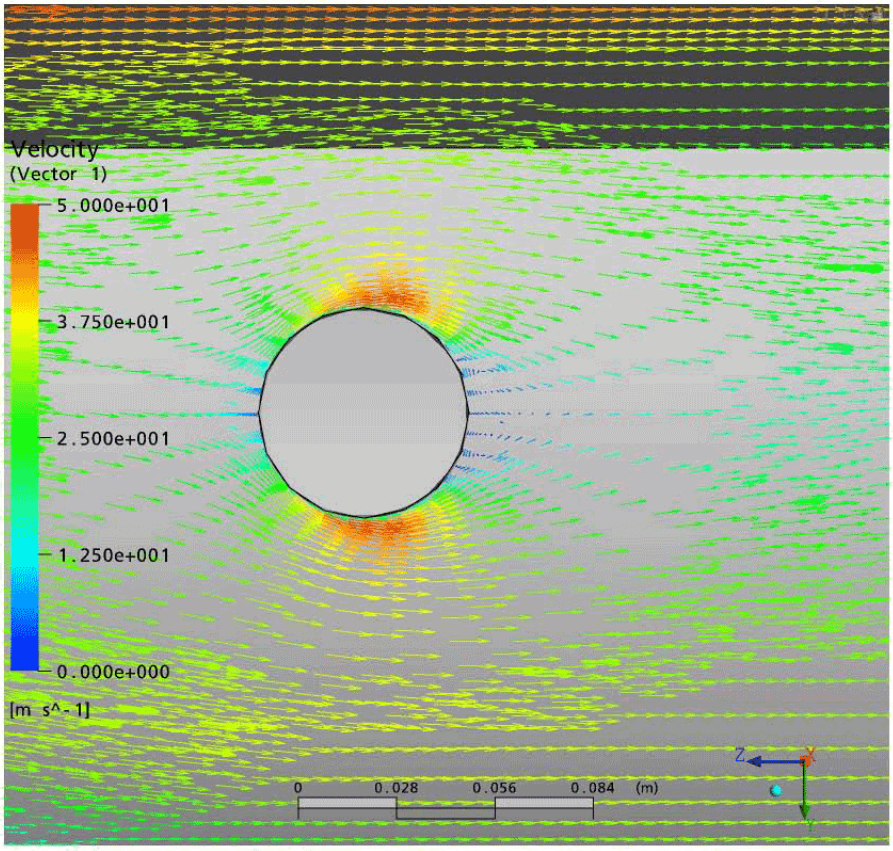


**Figure A3: Velocity Vector Plot near conduit at R=0.4m.**

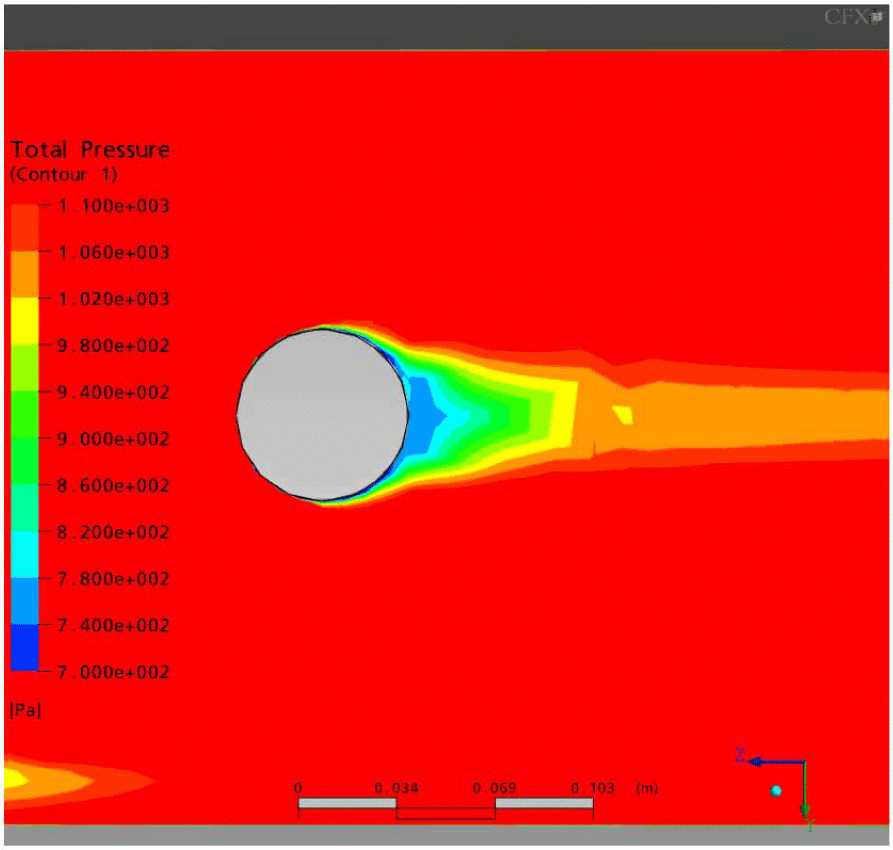


**Figure A4: Total pressure plot near conduit at R=0.4m.**

## APPENDIX B: Details of the Computational Model

The CFX 10.0 software consists of three components. These are:

**CFX Pre**: A general purpose CFD pre-processor for model set up, specification of boundary and initial conditions, and selection of solver options.

**CFX 10.0 Solver**: The CFD flow solver.

**CFX Post**: A general purpose CFD post-processor used for computing the quantitative measurements and creating the plots.

CFX 10.0 solves the three-dimensional Reynolds-averaged Navier-Stokes equations using a collocated, finite volume, primitive variables (Cartesian components of velocity) approach. It is applicable to flows ranging from fully incompressible to transonic to supersonic. The flow code is a hybrid finite element—finite volume method in the sense that a finite element assembly procedure is used to assemble conservative finite volume equations. The equations are discretised using a scheme known as High-Order Numerical Advection Correction. This discretisation scheme is formally second order accurate, and has very low levels of false diffusion with excellent conservation of stagnation quantities (total pressure and temperature). CFX 10.0 computes dynamic pressure (thermodynamic less hydrostatic). Turbulence was modeled with the standard two-equation k-ε model with scalable wall functions. The discrete linearised algebraic equations are solved using a powerful multi-grid method known as Additive Correction Multi-grid. Due to this multi-grid method, solution costs are observed to increase only linearly with increase in grid size.

### Hardware

Calculations were performed on Intel and AMD Athlon workstations running Linux.

## APPENDIX C: Sources of Error

The computed results will not precisely correspond to the real flow situation for a number of reasons. Five such reasons are:

1. Geometric representation.
2. Specification of boundary conditions.
3. Discretisation error.
4. Round-off error.
5. Modeling error.

A brief discussion of each of these items is provided below.

**Geometric representation**

The modeled flow can only hope to approach the real flow situation if the modeled geometry and applied boundary conditions correspond to reality. The precision of the geometric representation is limited by the finite amount of geometric data available. The geometry and grid were constructed based on geometric information, supplied by drawings. It is believed that the computational mesh employed in the calculations is sufficiently fine to represent the gross features of the supplied data.
Certain aspects of the geometry that were omitted from the computational model were:

- The gap between the blade and the hub.
- The gap between the fan and stator section.
- The fan hub was extended slightly so that the entire blade would lie on the hub surface. The actual design contains a blade that extends beyond the hub.
- Manufacturing tolerances and imperfections were also not considered.

**Specification of Boundary Conditions**

The walls were considered to be smooth, no slip walls. In reality, each component had various types and sizes of surface roughness. It is believed that the approximation introduced will have a marginal effect on the predicted values, but that it will not significantly affect the predicted flow patterns.

**Discretisation Error**

Discretisation error exists due to the fact that numerical methods employ a discrete, rather than a continuous, representation of the governing equations of fluid flow. This discretisation error diminishes as the grid density is increased. Three points are worthy of special consideration. First, the CFX code is numerically fully (and strongly) conservative. It therefore has the desirable property that mass is exactly conserved, even on coarse grids. Second, the discretisation technology employed in CFX software has been designed to exhibit relatively low levels of error

on coarse grids. Third, the discretisation used is second order in nature, and hence second order convergence with grid refinement is expected.

**Round-off Error**

The CFX code primarily uses single precision arithmetic (32-bit word). All solutions presented in this report were obtained by iterating the equations close to the round-off limit of the machine. Because the word-length is finite, the round-off error is also finite. Large grid aspect ratios can increase sensitivity to round-off errors.

**Modeling Error**

Modeling error arises from various assumptions, the largest one being associated with the turbulence model. CFX software employs the standard k-ε turbulence model, as well as the SST turbulence model. Many assumptions are made in the derivation of this model, but it is known to be of reasonable accuracy for mildly accelerating, attached flows. It is at present the turbulence model that is most generally applicable to a wide variety of flow situations. It is used in most commercially available CFD codes. Other more advanced turbulence models are under development, but they have not yet been proven for a wide range of flow situations.